HHS Public Access

Author manuscript

Nat Cell Biol. Author manuscript; available in PMC 2017 March 01.

Published in final edited form as:

Nat Cell Biol. 2016 September ; 18(9): 954–966. doi:10.1038/ncb3396.

Nuclear GSK3β promotes tumorigenesis by phosphorylating KDM1A and inducing its deubiquitination by USP22

Aidong Zhou[#1], **Kangyu Lin**[#1], **Sicong Zhang**[1,4], **Yaohui Chen**[1], **Nu Zhang**[5], **Jianfei Xue**[1], **Zhongyong Wang**[1], **Kenneth D. Aldape**[2,6], **Keping Xie**[3,4], **James R. Woodgett**[7], and **Suyun Huang**[1,4,9]

[1]Department of Neurosurgery, The University of Texas MD Anderson Cancer Center, Houston, Texas, USA

[2]Department of Pathology, The University of Texas MD Anderson Cancer Center, Houston, Texas, USA

[3]Department of Gastroenterology, Hepatology & Nutrition, The University of Texas MD Anderson Cancer Center, Houston, Texas, USA

[4]Cancer Biology Program, The University of Texas Graduate School of Biomedical Sciences at Houston, Houston, Texas, USA

[5]Department of Neurosurgery, The First Affiliated Hospital of Sun Yat-sen University, Guangzhou, Guangdong, People's Republic of China

[7]Samuel Lunenfeld Research Institute, Mount Sinai Hospital, Toronto, Ontario, Canada

[#] These authors contributed equally to this work.

Abstract

Emerging evidences have shown that GSK3β plays oncogenic roles in multiple tumor types; however, the underlying mechanisms remain largely unknown. Herein, we show that nuclear GSK3β is responsible for the accumulation of the histone demethylase KDM1A and critically regulates histone H3K4 methylation during tumorigenesis. GSK3β phosphorylates KDM1A serine 683 upon priming phosphorylation of KDM1A serine 687 by CK1α. Phosphorylation of KDM1A induces its binding with and deubiquitination by USP22, leading to KDM1A stabilization. GSK3β and USP22-dependent KDM1A stabilization is required for the demethylation of histone H3K4, thereby repression of *BMP2*, *CDKN1A*, and *GATA6* transcription, cancer stem cell self-renewal,

[9]Correspondence should be to address to S.H. (suhuang@mdanderson.org).

[6]Current address: MacFeeters-Hamilton Brain Tumour Centre, Princess Margaret Cancer Centre, University of Toronto, Toronto, Ontario, Canada

AUTHOR CONTRIBUTIONS

S.H. and A.Z. conceived of the project and designed the study; A.Z., K.L. performed most of the experiments under the supervision by S.H.; S.Z. and Y.C. assisted in some *in vitro* experiments; J.X. and Z.W. assisted in the mouse experiments; N.Z., K.A., K.X., and J.W. provided reagents and conceptual advice; S.H. and A.Z. wrote the manuscript. All authors discussed the results and commented on the manuscript.

COMPETING FINANCIAL INTERESTS

The authors declare no competing financial interests.

and glioblastoma tumorigenesis. In human glioblastoma specimens, KDM1A levels are correlated with nuclear GSK3β and USP22 levels. Furthermore, a GSK3 inhibitor tideglusib sensitizes tumor xenograft to chemotherapy in mice via KDM1A down-regulation and improves survival. Our findings demonstrate that nuclear GSK3β and USP22-mediated KDM1A stabilization is essential for glioblastoma tumorigenesis.

Glycogen synthase kinase 3 (GSK3) exists as two isoforms (α and β) that play central roles in many cellular and physiological processes[1, 2]. In mice, knockout of GSK3β leads to death prior to or at birth, and embryonic fibroblasts derived from GSK3β-null animals are sensitized to apoptosis[3]. In malignancies, GSK3β functions are tumor type–specific[4-6]. GSK3β was recognized as tumor suppressor by inactivating growth-promoting pathways such as those mediated by β-catenin and c-Myc proteins[7,8]. However, growing evidence indicates that GSK3β has tumor-promoting roles in diverse cancers, such as bladder cancer[6], osteosarcoma[9], leukemia[5], and glioblastoma[10]. Moreover, high nuclear GSK3β level has been associated with high-grade tumors and poor prognosis[6, 11, 12], and growth factors induce GSK3β nuclear translocation[13]. However, the roles and underlying mechanisms for nuclear GSK3β in tumorigenesis remain largely unknown.

Histone methylation plays an important role in the dynamic transitions of chromatin structure and critically regulates gene transcription, which contribute to tumor progression[14]. It has been shown that GSK3 is involved in the regulation of histone methylation including H3K4 methylation in the promoter regions of multiple genes[12, 15]. However, the molecular mechanisms for GSK3 in mediating alterations of histone methylation remain to be defined.

Lysine-specific histone demethylase 1A (KDM1A/LSD1) is the first identified lysine-specific histone demethylase. As a key component of various transcriptional co-repressor complexes, KDM1A selectively removes the methyl from H3K4me1/2 and mediates gene repression[16, 17]. During cell cycle progression, KDM1A is hyperphosphorylated in tumor cells by an unknown mechanism[18]. Moreover, like GSK3β, the function of KDM1A shows tumor type specificity. In breast carcinomas, KDM1A is downregulated and introduction of KDM1A inhibits cancer metastatic potential *in vivo*[17]. In contrast, KDM1A was elevated in a variety of cancers[19-21], including glioblastoma[22], and plays important roles in tumor progression[22, 23]. Until now, the mechanisms that lead to KDM1A dysregulation in these tumors remain unclear.

In this report, we have found that high-level nuclear GSK3β is responsible for the accumulation of KDM1A by inducing it's binding with and deubiquitination by USP22. We have demonstrated that the GSK3β-USP22-KDM1A axis is critical for gliomagenesis and targeting GSK3β-USP22-KDM1A axis is a potential therapeutic strategy against glioblastoma.

RESULTS

GSK3β stabilizes KDM1A protein by decreasing its ubiquitination

We first assessed the relationship between GSK3β and KDM1A because both have been associated with malignancy in glioblastoma and other tumors[20, 21, 23]. We found that both

nuclear GSK3β and KDM1A are highly expressed in glioblastoma cell lines, especially in glioma stem cells (GSCs) as compared with non-GSC glioma cell lines[24], and that their expression levels were directly correlated (Fig. 1a). We next assessed KDM1A levels in GSK3β wild-type ($GSK3\beta^{+/+}$) and GSK3β knockout ($GSK3\beta^{-/-}$) mouse embryonic fibroblasts (MEFs) and found that KDM1A expression was sharply decreased after GSK3β knockout, but rescued by reconstituted expression of GSK3β (Fig. 1b and Supplementary Fig. 1a). Likewise, KDM1A levels were elevated by wild-type GSK3β (GSK3β-WT) or constitutively active GSK3β (GSK3β-CA), but not by kinase-defective GSK3β (GSK3β-KD) (Fig. 1c). In contrast, KDM1A levels in GSK3β siRNA-transfected GSC11 cells were lower than those in control cells (Supplementary Fig. 1b). Knockdown of GSK3α, the other GSK3 isoform, also decreased KDM1A levels but to a lesser degree (Supplementary Fig. 1c), suggesting partial redundancy with GSK3β playing the major role. However, we found no difference in KDM1A mRNA levels between $GSK3\beta^{+/+}$ and $GSK3\beta^{-/-}$ MEFs (Supplementary Fig. 1d). Moreover, there is no difference in KDM1A levels between β-catenin knockout and β-catenin wild-type MEFs (Supplementary Fig. 1e), indicating that GSK3β regulates KDM1A independent of Wnt/β-catenin signaling.

KDM1A has been reported to be subject to proteasome degradation[16], and we confirmed this result (Supplementary Fig. 1f). In GSC11, the proteasome inhibitor MG132 reversed the inhibiting effect of GSK3β knockdown on KDM1A (Fig. 1d). Furthermore, KDM1A stability was decreased in $GSK3\beta^{-/-}$ MEFs compared with that in $GSK3\beta^{+/+}$ MEFs (Fig. 1e). Likewise, knockdown of GSK3β in GSC11 cells promoted KDM1A degradation (Fig. 1f). These results were confirmed in 293T cells transfected with control vector or GSK3β-CA (Supplementary Fig. 1g). We next performed the immunofluorescence-based co-expression assays in glioblastoma specimens. The results showed that the percentages of nuclear GSK3β/KDM1A double-stained cells are significantly higher than that of nuclear GSK3β negative but KDM1A positive cells (Fig. 1g,h, $p<0.001$), suggesting KDM1A co-expresses with nuclear GSK3β in tumor cells.

We assessed the effect of GSK3β on the ubiquitination of KDM1A. Compared with control vector, transfection of GSK3β-WT and GSK3β-CA greatly inhibited KDM1A ubiquitination in the presence of MG132, whereas GSK3β-KD almost had no effect (Fig. 1i). Moreover, knockdown of GSK3β in GSC11 cells increased KDM1A ubiquitination (Fig. 1j). Together, these results support the notion that GSK3β stabilizes KDM1A by decreasing its ubiquitination.

GSK3β phosphorylates KDM1A serine 683 after priming phosphorylation by casein kinase Iα

KDM1A's amino acid sequence contains several potential GSK3β phosphorylation sites harboring a canonical -S/T×××S/T- motif (Fig. 2a and Supplementary Fig. 2a). Lithium chloride (a GSK3 inhibitor) treatment decreased the level of phospho-serine/threonine on KDM1A in GSC11 cells (Fig. 2b). Moreover, GSK3β is localized in both the cytoplasm and nucleus and co-localized with KDM1A in the nuclei in glioblastoma cells and GSCs (Supplementary Fig. 2b). Furthermore, nuclear GSK3β and KDM1A bound to each other in

GSC11 cells (Fig. 2c), and KDM1A's amine oxidase-like (AOL) domain (residues 522-852) is required for KDM1A's binding with GSK3β (Fig. 2d).

To identify the target sites of GSK3β, we mutated Ser/Thr to Ala at Ser-31, Thr-389, Thr-542, Thr-607, Ser-683, or Ser-781 of KDM1A. Mutation of Ser-683 to Ala (S683A) increased ubiquitination and degradation of KDM1A (Supplementary Fig. 2c,d). In contrast, mutation of Ser-683 to Asp (S687D), which mimics Ser-683 phosphorylation, stabilized KDM1A (Supplementary Fig. 2d). These results, which are in line with our finding that GSK3β binds to residues 522–852 (Fig. 2d), indicate that Ser-683 may be phosphorylated by GSK3β and is required for the regulation of KDM1A ubiquitination.

Substrate phosphorylation by GSK3β usually requires a prior phosphorylation by a priming kinase to form the -S/T×××pS/T- motif. Amino acid sequence analysis predicts with high probability that Ser-687 is phosphorylated by casein kinase 1 (CK1) (Fig. 2a). Moreover, treatment of GSC11 and HFU-251 MG cells with D4476, a CK1 inhibitor[25], potentiated lithium chloride's repression on KDM1A expression (Supplementary Fig. 2e). Using tagged proteins ectopically expressed in 293T cells or endogenous proteins from GSC11 cells, we found that KDM1A interacts with CK1α, but not with CK1δ or CK1ε (Fig. 2c and Supplementary Fig. 2f,g). Furthermore, KDM1A levels are decreased only by knockdown of CK1α, but not other CK1 isoforms (Supplementary Fig.2h).

We next performed *in vitro* kinase assays and found that GSK3β phosphorylated wild-type KDM1A in the presence of CK1α, but not in its absence (Fig. 2e). However, we did not detect phosphorylation using the S683A/S687A mutant (Fig. 2e). Moreover, using a specific antibody against phospho-KDM1A Ser-683 (p-KDM1A-S683), we only detected KDM1A phosphorylation in 293T cells transfected with wild-type KDM1A, but not KDM1A S683A (Fig. 2f, lane 2 *vs* lane 4). In addition, the p-KDM1A-S683 level was upregulated by GSK3β-CA in the cells transfected with wild-type KDM1A, but not KDM1A S683A (Fig. 2f). Furthermore, endogenous p-KDM1A-S683 was detected in GSC11 and HF-U251-MG cells, whereas inhibition of GSK3β or CK1 decreased endogenous p-KDM1A-S683 levels (Fig. 2g). These results consistently indicated that priming phosphorylation by CK1α at Ser-687 facilitates GSK3β phosphorylation of KDM1A Ser-683, which then represses KDM1A ubiquitination.

GSK3β-dependent phosphorylation of KDM1A promotes KDM1A's deubiquitination and stabilization by ubiquitin-specific protease 22

Because Ser-683 phosphorylation decreased KDM1A ubiquitination, we hypothesized that GSK3β functions in cooperation with an unknown deubiquitinase (DUB) to deubiquitinate KDM1A. We therefore screened a panel of DUBs in which 23 DUBs' cDNA plasmids were transfected into 293T cells, and found that USP15, USP21, USP22, and USP28 upregulated KDM1A levels (Supplementary Fig. 3a). However, of those four DUBs, only USP22 substantially decreased KDM1A ubiquitination (Supplementary Fig. 3b-d). This result was further confirmed under denaturing conditions (Fig. 3a). Moreover, using *in vitro* deubiquitination assay, we found that KDM1A ubiquitination was decreased by incubating with recombinant USP22, suggesting that USP22 deubiquitinates KDM1A directly (Fig. 3b).

Furthermore, knockdown of USP22 in GSC11 cells increased KDM1A ubiquitination (Fig. 3c).

We next assessed the effect of USP22 on KDM1A stability. In GSC11 cells, USP22 knockdown decreased KDM1A protein level (Fig. 3d), but not KDM1A mRNA (Supplementary Fig.3e). Down-regulation of KDM1A protein by USP22 knockdown was due to the decreased KDM1A stability (Fig. 3e). In contrast, USP22 overexpression in 293T cells increased KDM1A stability (Supplementary Fig. 3f). Moreover, in a panel of cell lines, the levels of nuclear USP22 and KDM1A were directly correlated (Fig. 3f and Supplementary Fig. 3g). The levels of nuclear GSK3β and KDM1A were also directly correlated in most of the cell lines (Fig. 3f and Supplementary Fig. 3g). Furthermore, in GSCs, KDM1A and USP22 were co-localized in nuclei (Supplementary Fig. 3h). In glioblastoma specimens, the percentages of nuclear USP22/KDM1A double-stained cells are significantly higher than that of nuclear USP22 negative but KDM1A positive cells (Fig. 3g, h, $p<0.001$), suggesting nuclear KDM1A co-expresses with USP22 in tumor cells. These results indicate that USP22 deubiquitinates and stabilizes KDM1A.

We sought to determine whether KDM1A's deubiquitination by USP22 depends on KDM1A's phosphorylation by GSK3β. Using a series of KDM1A deletion mutants, we found that KDM1A's AOL domain was required for KDM1A's binding with USP22 (Fig. 4a). Coincidentally, KDM1A's AOL domain was required for KDM1A's binding with GSK3β (Fig. 2d), suggesting a possible link between KDM1A phosphorylation and deubiquitination. Moreover, GSK3β knockdown in GSC11 cells attenuated the interaction between endogenous USP22 and KDM1A (Fig. 4b), which was confirmed in 293T cells by transfection of GSK3β-KD as compared with GSK3β-CA (Supplementary Fig. 4). In addition, deubiquitination of KDM1A by USP22 was attenuated after GSK3β knockdown (Fig. 4c). Furthermore, KDM1A S683A significantly decreased the interaction between USP22 and KDM1A in the presence of GSK3β-CA (Fig. 4d). Accordingly, the mutation also attenuated KDM1A's deubiquitination by USP22 in the presence of GSK3β-CA (Fig. 4e). These results demonstrate that GSK3β-dependent phosphorylation of KDM1A is critical for KDM1A's binding with and deubiquitination by USP22.

GSK3β and USP22 regulate KDM1A target gene expression and maintain the stemness of GSCs through KDM1A

KDM1A has been reported to regulate a series of genes associated with cell proliferation, stem cell pluripotency and differentiation, including *BMP2*, *CDKN1A,* and *GATA6*[26, 27]. In GSCs, knockdown of KDM1A, GSK3β and USP22 decreased KDM1A's binding to the promoter of those target genes (Supplementary Fig. 5a). Moreover, KDM1A knockdown increased H3K4me2 as well as the permissive H3K4me3 levels in the promoters of *BMP2*, *CDKN1A,* and *GATA6* (Fig. 5a), and this led to the increased levels of their mRNAs and proteins (Fig. 5b,c). Knockdown of GSK3β or USP22 also led to the accumulation of both H3K4me2 and H3K4me3 levels in *BMP2*, *CDKN1A,* and *GATA6* promoters (Fig. 5a), and decreased their mRNA and protein levels (Fig. 5b,c), suggesting that GSK3β and USP22 epigenetically repress the expression of those genes via KDM1A.

We further investigated the roles of KDM1A in regulating GSC stemness. Knockdown of KDM1A in GSCs decreased the frequency of neurosphere formation as determined by limited dilution assays (Fig. 5d and Supplementary Fig. 5b), and decreased the sphere formation efficiency as determined by primary and secondary neurosphere assays (Supplementary Fig. 5c, j). Moreover, upon KDM1A knockdown, stem cell markers Nestin, Oct4, and CD133 were decreased, whereas the differentiation marker Tuj1 was increased (Fig. 5e and Supplementary Fig. 5d,e). Furthermore, shRNA-resistant KDM1A rescued the effect of sh-KDM1A on GSC stemness (Fig. 5d,e and Supplementary Fig. 5f). Likewise, knockdown of USP22 inhibited GSC stemness (Fig. 5d,f and Supplementary Fig. 5g), and exogenous KDM1A rescued the effect of USP22 depletion on GSC stemness (Fig. 5d,f and Supplementary Fig. 5g). These results suggest that USP22 promotes the stemness of GSCs through KDM1A.

In GSC11 cells, knockdown of GSK3β inhibited the expression of the stem cell markers but increased the expression of the differentiation marker (Fig. 5g and Supplementary Fig. 5h), and substantially decreased the frequency and efficiency of sphere formation (Fig. 5h,i and Supplementary Fig. 5j). We next overexpressed KDM1A S683D or S683A in GSK3β-depleted cells. Although KDM1A mRNA levels were similar in KDM1A S683D and S683A transfected cells (Supplementary Fig. 5i), only KDM1A S683D overexpression greatly increased the KDM1A protein in GSK3β-depleted cells (Fig. 5g). Moreover, the inhibitory effect of GSK3β depletion on GSC stemness was rescued by KDM1A S683D, but not S683A (Fig. 5g-i and Supplementary Fig. 5j). These results suggest that the GSK3β-dependent phosphorylation of KDM1A is important for maintaining the stemness of GSCs.

GSK3β and USP22 promote the tumorigenicity of GSCs through KDM1A

Using a mouse model, we investigated whether GSK3β and USP22 regulate the tumorigenicity of GSCs through KDM1A. All mice intracranially injected with control GSC11 cells developed tumors with characteristic glioblastoma features (Fig. 6a). In contrast, depletion of KDM1A in GSC11 cells abrogated brain tumor formation, which was rescued by KDM1A-shR (Fig. 6a). Likewise, depletion of USP22 in GSC11 cells abrogated brain tumor formation (Fig. 6a), but the inhibitory effects of USP22 depletion was rescued by KDM1A expression (Fig. 6a).

We next determined the role of GSK3β-dependent phosphorylation of KDM1A at S683 in promoting tumorigenesis. GSK3β depletion in GSC11 cells almost abrogated brain tumor formation (Fig. 6b). Moreover, the inhibitory effect of GSK3β depletion on tumorigenicity was rescued by KDM1A S683D, but not S683A (Fig. 6b). Immunohistochemical analysis showed that KDM1A expression in GSK3β-depleted tumor was recovered by KDM1A S683D, but not by S683A (Supplementary Fig. 6). These results suggest that GSK3β-dependent phosphorylation of KDM1A is necessary for promoting the tumorigenicity of GSCs.

KDM1A expression is correlated with nuclear GSK3β and USP22 expression in human glioblastoma specimens, and nuclear GSK3β/USP22/KDM1A expression is associated with grade of glioma malignance

To determine the potential clinical relevance of our findings, we assessed the expression of GSK3β, USP22, and KDM1A proteins in serial sections of 95 human glioblastoma (WHO grade IV) specimens. Expression levels of KDM1A were significantly correlated with those of nuclear GSK3β and USP22 (Fig. 6c, Fig. 6d: upper panel, r=0.6048, P<0.0001; lower panel, r=0.6784, P<0.0001). We next examined whether the levels of nuclear GSK3β, USP22, and KDM1A correlated with the grade of glioma malignance using the same 95 glioblastomas specimens with 50 low-grade astrocytomas (WHO grade II) specimens. The levels of nuclear GSK3β, USP22, and KDM1A were significantly lower in the 50 astrocytomas than in the 95 glioblastomas (Fig. 6e). These results strongly suggest that dysregulated KDM1A expression in glioblastoma is driven by high-level nuclear GSK3β and USP22.

The GSK3 inhibitor tideglusib attenuates the tumor-initiating ability of GSCs and sensitizes GSCs-derived glioblastoma xenografts to TMZ in mice

We next assessed the effect of GSK3β inhibition on GSCs. Tideglusib is an irreversible and non–adenosine triphosphate (ATP)-competitive GSK3 inhibitor[28]. Tideglusib treatment of GSC11 cells decreased the level of phosphorylated tau, a well-established GSK3β target (Supplementary Fig. 7a). Tideglusib was reported to increase the level of phosphorylated GSK3β-S9[29, 30], which was also found in GSC11 cells (Fig. 7a). Moreover, tideglusib treatment repressed KDM1A (Fig. 7a), which confirmed our finding that GSK3β stabilizes KDM1A. Furthermore, because it decreased CD133, Nestin, and Oct4 expression but increased Tuj1 expression, tideglusib treatment led to the loss of GSC features (Fig. 7b and Supplementary Fig. 7b). Tideglusib also attenuated GSC neurosphere formation (Fig. 7c,d). Importantly, tideglusib was not toxic to normal human astrocytes (Supplementary Fig. 7c).

In glioblastoma, GSCs are believed to be the main cause of temozolomide (TMZ) resistance[31]. Therefore, we sought to determine whether tideglusib inhibits GSC self-renewal to sensitize GSCs to TMZ. Tideglusib significantly repressed GSC viability and sensitized the cells to TMZ treatment *in vitro* (Fig. 7e, f). Given the good blood-brain barrier penetration and excellent *in vivo* tolerability of tideglusib, we next assessed the effects of tideglusib alone, TMZ alone, and tideglusib plus TMZ on the tumorigenicity of GSCs (Supplementary Fig. 7d). TMZ alone had little effect on tumor formation (Fig. 8a). However, tideglusib alone significantly decreased the tumor size, and tideglusib plus TMZ almost abrogated tumor formation (Fig. 8a). Moreover, tideglusib increased the levels of pGSK3β--S9 and Tuj1 but decreased the KDM1A and CD133 in tumors (Fig. 8b), suggesting that tideglusib inhibits tumorigenicity by inhibiting the stemness of GSCs through the GSK3β-KDM1A axis.

Next, we assessed the effects of tideglusib alone, TMZ alone, and tideglusib plus TMZ on the on the survival of GSC11- or GSC20-glioblastoma-bearing mice. TMZ alone had a modest effect on survival (Fig. 8c), and tideglusib alone had a better effect on survival than TMZ alone (Fig. 8c). However, TMZ plus tideglusib significantly improved the survival of

the GSCs-glioblastoma–bearing mice as compared with TMZ or tideglusib alone (Fig. 8c). Certainly, TMZ combined with tideglusib significantly extended overall survival of GSC11-glioblastoma–bearing mice as compared with no-treatment control (median survival duration of 83 d *vs.* 49 d) as well as survival of GSC20-glioblastoma–bearing mice (89 d *vs.* 58 d) (Fig. 8c). Together, these results indicate that tideglusib sensitizes GSCs-derived xenografts to TMZ and support clinical application of this combinatorial targeted therapy for treatment of glioblastoma.

DISCUSSION

In this study, we have identified a critical role for GSK3β in KDM1A accumulation via phosphorylating KDM1A and thus enhancing KDM1A's binding with and deubiquitination by USP22, which leads to GSC self-renewal and glioblastoma tumorigenesis (Fig. 8d). Our mechanistic and clinical findings establish that GSK3β-USP22-KDM1A axis is critical for glioblastoma tumorigenesis and targeting this axis is a potential therapeutic strategy against glioblastoma.

The function of GSK3β in malignancy is affected by the context with substrate as well as tumor type. GSK3β phosphorylates a series of substrates, including β-catenin[32] and Myc[33], which leads to their degradation and/or inactivation, thus inhibiting signals that would otherwise promote cell proliferation and self-renewal. On the other hand, GSK3β also promotes cell survival by activating multiple pro-proliferative pathways or factors, including mammalian target of rapamycin (mTOR)[34], nuclear factor κB (NF-κB)[3, 35], STAT3[36], and C/EBPβ[37]. Interestingly, GSK3 inhibition leads to NF-κB target gene repression partially by affecting histone methylation of the target promoters[12]. Our present study has strongly suggested that the GSK3β-USP22-KDM1A axis may underlie this action. Moreover, GSK3β-mediated phosphorylation of substrates also stabilize target proteins by an unknown mechanism[38, 39]. Our present study identified that KDM1A phosphorylation by GSK3β promotes KDM1A's binding with and then deubiquitination by USP22, which provides a direct link between substrates phosphorylation and deubiquitination.

As a reverse procedure of ubiquitination, protein deubiquitination is a highly controlled process[28]. Recent studies reported that phosphorylation of the deubiquitinase OTULIN negatively regulates its interaction with HOIP and thus promotes HOIP ubiquitination[40, 41]. In the current study, we found that substrate phosphorylation affects its recognition by a DUB. Specifically, KDM1A phosphorylation by GSK3β increases KDM1A's association with and then deubiquitination by USP22. In contrast, USP28, a previously identified DUB for KDM1A in breast cancer cells[42], did not substantially affect KDM1A ubiquitination in our system. Furthermore, previous studies show that USP22 is involved in the regulation of cancer stem cell and required for tumor progression in some cancers[43]. So far, only a few substrates of USP22 have been identified[43, 44], and little is known about USP22's functions in GSCs and glioma tumorigenesis. Our present study demonstrates that USP22 is highly expressed in glioblastoma, and USP22 knockdown suppresses the stemness and tumor-initiating ability of GSCs.

Tideglusib is a selective non-ATP-competitive GSK3 inhibitor with good blood-brain barrier penetration and now in a phase II trial for the treatment of Alzheimer disease[28, 45]. Our study demonstrates that tideglusib has potent therapeutic efficacy against glioblastoma in a preclinical model. Specifically, tideglusib inhibits GSC self-renewal and sensitizes glioblastoma to TMZ *in vivo* but has little effect on the proliferation of normal astrocytes. The tumor specificity of tideglusib may be due to the elevated nuclear GSK3β levels in glioblastoma cells, which leads to upregulation of KDM1A target tumor suppressors. Of these targets, BMP2 sensitizes glioblastoma stem-like cells to TMZ by inhibiting hypoxia-inducible factor 1α stability[46]. GATA6 is a differentiation marker and inhibits the tumorigenicity of glioblastoma cells[47]. CDKN1A is an inhibitor of glioma stem cell proliferation[48], and is involved in determining the fate of glioblastoma cells after TMZ treatment[49].

In conclusion, we show that GSK3β phosphorylates and stabilizes KDM1A by promoting recruitment of USP22, leading to repression of KDM1A target genes. Moreover, disruption of GSK3β-USP22-KDM1A axis by tideglusib represses glioma tumorigenesis, sensitizes glioblastoma xenografts to TMZ treatment, and improves mouse survival, suggesting a potential therapeutic strategy against glioblastoma.

METHODS

Regents and Antibodies

Antibodies against human KDM1A (ab17721 and ab90966), CK1δ (ab48031), GATA6 (ab22600), and USP22 (ab4812) were from Abcam. Antibodies against GST (sc-138), Tuj-1(sc-58888), CK1α (sc-6477), CK1ε (sc-6471), BMP2 (sc-6895), CDKN1A (sc-397), and α-Tubulin (sc-5286) were from Santa Cruz Biotechnology. Antibodies against human GSK3β (9315), GSK3α (9338), CD133 (3663), phospho-GSK3β-S9 (9336), Oct4 (2750), H3K4me2/3 (9725 and 9751) and Myc-tag (2276) were from Cell Signaling Technology. Antibodies against phospho-serine/threonine (612548) and nestin (611658) were from BD Transduction Laboratories. Antibodies against hemagglutinin (HA)-Tag and Flag-tag were from Sigma. Hoechst 33342, Alexa Fluor 488 goat anti-rabbit antibody, and Alexa Fluor 594 goat anti-mouse antibody were from Molecular Probes. The specific antibody against phospho-KDM1A S683 was produced by Signalway Antibody. Supplementary Table 1 contains detailed information about the used antibodies.

Temozolomide (TMZ), tideglusib, lithium chloride, glutathione S-transferase (GST) beads, cycloheximide (CHX), and MG132 were from Sigma. Puromycin, hygromycin, and D4476 (4-[4-(2,3-dihydro-benzo[1,4]dioxin-6-yl)-5-pyridin-2-yl-1*H*-imidazol-2-yl] benzamide) were from EMD Biosciences. Protein G agarose was from Life Technologies. The recombinant active GSK3β (G09-10G) and CK1α (C64-10G) proteins were from SignalChem Lifesciences Corp.

shRNA and siRNA

Lentiviral shRNA plasmids were from Sigma. The shRNAs against human KDM1A (*NM_015013*) correspond to the coding sequences (CDSs) from 1311 to 1332 (KDM1A-

sh1, TRCN0000046071) and from 1975 to 1995 (KDM1A-sh2, TRCN0000046072) relative to the first nucleotide of the start codon. The shRNAs against human USP22 (*NM_015276*) correspond to the CDSs from 545 to 565 (USP22-sh1, TRCN0000296868) and from 1366 to 1385 (USP22-sh2, TRCN0000296867). The shRNA against human GSK3β (*NM_002093*) correspond to the CDSs from 1838 to 1848 (GSK3β-sh1, TRCN0000039999) and from 1058 to 1078 (GSK3β-sh2, TRCN0000039564). The siRNAs against USP22 and GSK3β have the same target sequences as the shRNAs respectively. All siRNAs were synthesized by Sigma. Supplementary Table 2 contains detailed information about the siRNA sequence.

Cell culture, transfection, and treatment

NHAs-E6/E7 (normal human astrocytes immortalized with human telomerase reverse transcriptase and infected with retrovirus E6/E7), MEFs, and 293T, 293FT, LN229, HFU251, HS683, SW1783, and U87 cells were cultured in Dulbecco's modified Eagle's medium supplemented with 10% bovine calf serum (HyClone). GSC11, GSC20, GSC23, and GSC262 human GSCs isolated from human glioblastoma specimens were described previously[27], and were maintained in a 50:50 mixture of Dulbecco's modified Eagle's medium and F-12 medium supplemented with B27, epidermal growth factor (10 ng/ml), and basic fibroblast growth factor (10 ng/ml). Only early-passage GSC cells were used for the study. No cell lines used in this study were found in the database of commonly misidentified cell lines that is maintained by ICLAC and NCBI Biosample. Cell lines were authenticated by short tandem repeat profiling and were routinely tested for mycoplasma contamination.

Transfections of plasmids and siRNAs were performed using X-tremeGENE HP and X-tremeGENE siRNA transfection reagents (Roche), respectively. The standard concentrations of the following inhibitors for cell treatment are: cycloheximide (CHX), 50 μg/mL; MG132, 20 μM; D4476, 20 μM; lithium chloride (LiCl), 20 mM.

Plasmid constructs and mutagenesis

USP2, USP4, USP5, USP8, USP13, USP14, USP16, USP18, USP25, USP26, USP29, USP30, USP36, USP39, USP46, and USP48 expression plasmids were kindly provided by Dr. Jianhua Yang (Texas Children's Cancer Center). Flag-HA-USP1, USP3, USP21, USP22, and CYLD were kindly provided by Dr. Hui-Kuan Lin (MD Anderson Cancer Center). Myc-USP11, Flag-USP15, and Flag-USP28 were from Addgene. Myc-GSK3β-WT, Myc-GSK3β-CA, and Myc-GSK3β-KD were kindly provided by Dr. Mien-Chie Hung (MD Anderson Cancer Center). Flag-KDM1A was kindly provided by Dr. Yang Shi (Harvard University). USP22 cDNA from Flag-HA-USP22 plasmid was further cloned into pcDNA3-HA vector and pGEX-4T-1 vector.

Deletion mutants of KDM1A were constructed into 3×Flag vector. Site-directed mutagenesis in KDM1A was introduced using the QuikChange site-directed mutagenesis kit (Agilent Technologies). GST-tagged KDM1A or KDM1A S683A/S687A was constructed by cloning the wild-type or mutant cDNA into pGEX-4T-1 (GE Healthcare). Lentiviral expression of KDM1A-shR, KDM1A S683D, or KDM1A S683A was achieved by cloning the cDNA into a pLVX-IRES-Hyg vector. The cDNAs of three CK1 isoforms were amplified and cloned

into pcDNA3-HA vector. All plasmids were confirmed by DNA sequencing. Supplementary Table 2 contains the detail information about the sequence of the used primers.

Generation of lentiviral stable cell lines

To generate lentiviral stable cells expressing shRNAs, we transfected 293FT cells in 60-mm dishes with pLKO.1-shRNA plasmids and the ViraPower Lentiviral Packaging Mix (Life Technologies). Twenty-four hours after transfection, the supernatant was collected, filtered, and used to infect GSCs cultured in 6-well plates. Thirty-six hours after infection, cells were selected with puromycin (10 μg/ml) for 1 week. For the generation of stable cells expressing KDM1A-shR, KDM1A S683D, or S683A, GSCs were transduced with lentivirus expressing KDM1A-shR, KDM1A S683D, or S683A cDNA and then selected by hygromycin (200 μg/ml) for 1 week.

Extreme limiting dilution assay and neurosphere formation

In vitro limiting dilution assay (LDA) was performed as described previously[50]. Briefly, GSCs expressing different constructs were dissociated to single cells and then plated in 96-well plates at a cell number of 1, 5, 10, or 25 cells per well. Wells with no neurosphere were counted for each group after 10 d. Extreme limiting dilution assays were analyzed using software available at http://bioinf.wehi.edu.au/software/elda/ [51]. Primary and secondary neurosphere assays were performed as we described previously[52]. Briefly, dissociated single cells were plated at a density of 1 cell/μl, and the spheres that formed after 10 d were counted. For secondary neurosphere assay, established tumorspheres were dissociated into single cells and plated at a clonal density of 1 cell/μl, and the spheres that formed after 10 d were counted.

Nuclear protein extraction, immunoprecipitation, and immunoblotting

Nuclear proteins were extracted using the CelLytica NuCLEAR Extraction Kit (Sigma) according to the manufacturer's instructions. The extraction of total proteins was performed using immunoprecipitation lysis buffer (25 mM Tris-HCl pH 7.4, 150 mM NaCl, 1% NP-40 nonyl phenoxypolyethoxylethanol, 1 mM ethylenediaminetetraacetic acid, protease and phosphatase inhibitors) or radioimmunoprecipitation assay buffer (50 mM Tris pH 8.0, 150 mM NaCl, 1% nonylphenoxypolyethoxyethanol, 0.1% sodium dodecyl sulfate [SDS], protease and phosphatase inhibitors), and immunoprecipitation or immunoblotting with corresponding antibodies was performed as described previously[52]. All experiments were independently repeated three times.

GST-Tagged protein purification

GST-KDM1A-WT, GST-KDM1A S683A/S687A, and GST-USP22 in the bacterial expression plasmid pGEX-4T-1 were expressed in *Escherichia coli* BL21 under 0.5 mM isopropyl β-d-1-thiogalactopyranoside at 16 °C. Cells were resuspended in BugBuster Protein Extraction Reagent (Novagene). The proteins were purified using glutathione beads (Sigma) according to the manufacturer's protocol.

In vitro kinase assay

The purified GST-KDM1A-WT or GST-KDM1A S683A/S687A fusion protein as a substrate was incubated with 10 ng of purified GSK3β and CK1α (SignalChem) in kinase assay buffer containing 2 μCi [γ-^{32}P]ATP per reaction. The kinase reaction was performed at 30 °C for 30 min, and the reaction was terminated by adding SDS sample buffer. The resultant product was then subjected to SDS–polyacrylamide gel electrophoresis and autoradiography.

In vivo and *in vitro* detection of KDM1A ubiquitination

Cells were co-transfected with the indicated plasmids for 48 h and then treated with the proteasome inhibitor MG132 (20 μM) for 6 h. Cells were lysed using RIPA lysis buffer [50 mM Tris-base pH 6.8, 150 mM NaCl, 1% NP-40, 0.5% deoxycholic acid, 0.1 % SDS, 10 mM NaF, 10 mM DTT, 0.2 mM Na_3VO_4, 1% cocktail protease inhibitors, 1 mM phenylmethylsulfonyl fluoride (PMSF)]. Cell lysates were immunoprecipitated using the indicated antibodies and washed for 3 times by RIPA buffer. To exclude non-specific ubiquitin-modified species from the KDM1A complex, we washed the immunoprecipitates for 3 times using a ubiquitination wash buffer [50 mM Tris base pH 6.8, 150 mM NaCl, 1% NP-40, 0.5 % deoxycholic acid, 1 M urea, 1 mM N-ethylmaleimide (NEM), and protease inhibitors][53].

In vitro deubiquitination of KDM1A by USP22 was performed as described previously[54]. HF-U251 MG cells were transfected with Flag-KDM1A and HA-Ubi expression vectors. After treatment by MG132 for 6h, KDM1A protein containing ubiquitinated KDM1A was purified from the cell lysates using Flag-beads and washed extensively using Flag-lysis buffer (50mM Tris-HCl pH 7.8, 137mM NaCl, 10mM NaF, 1mM EDTA, 1% Triton X-100, 0.2% Sarkosyl, 1mM DTT, and proteinase inhibitor cocktail). The proteins were then eluted with Flag-peptides (Sigma) in BC100 buffer (25mM Tris-HCl pH 7.8, 100mM NaCl). The recombinant GST-Tagged USP22 protein was expressed in BL21 cells and purified using GST beads. For the deubiquitination assay reaction *in vitro*, the ubiquitinated KDM1A protein was incubated with different amount of recombinant USP22 protein (10ng or 100ng) in a deubiquitination buffer (50mM Tris-HCl pH 8.0, 50mM NaCl, 1mM EDTA, 10mM DTT, 5% glycerol) for 2 h at 37 °C. The result reactions were subjected immunoblotting analysis.

In vitro cell viability assay

NHAs, GSC11 cells, or GSC20 cells in 96-well plates were treated with TMZ (100 μM), tideglusib (2.5 or 5 μM), or both tideglusib and TMZ for the indicated numbers of days. Cell viability was analyzed using an XTT assay kit (Sigma) according to the manufacturer's instructions.

Chromatin immunoprecipitation assay

Chromatin immunoprecipitation (ChIP) was performed as described previously[52]. Briefly, 2×10^6 cells were used for each reaction. The resulting precipitated DNA samples were used for the quantitative polymerase chain reaction (PCR) analysis.

Quantitative PCR

Total RNA was extracted using Trizol reagent (Invitrogen) and reverse-transcribed using the iScript™ Reverse Transcription Supermix (Bio-Rad) according to the manufacturer's instructions. The reverse-transcribed cDNA products were used for quantitative PCR analysis using SYBR Select Master Mix (Life Technologies). All quantitative PCR results were mean ± s.e.m. from three independent experiments. Supplementary Table 2 contains the detail information about the sequence of the used primers.

Immunohistochemical and Immunofluorescence analysis

Anonymous archived human glioma specimens (50 grade II astrocytomas and 95 glioblastomas) were obtained from The University of Texas MD Anderson Cancer Center under a protocol approved by the Institutional Review Board. All tissue samples were collected in compliance with informed consent policy. For antibody staining, tissue slides were deparaffinized, rehydrated through an alcohol series, and then stained with primary antibodies against human KDM1A (ab17721, Abcam), USP22 (ab4812, Abcam), phospho-GSK3β-S9 (9336), and GSK3β (9315, Cell Signaling Technology) using standard procedures[52]. To quantify GSK3β, KDM1A, and USP22 expression, we measured the immunostaining scores of GSK3β, KDM1A, or USP22 in human glioblastoma tissues as described previously[52]. Briefly, staining of nuclear GSK3β, KDM1A, or USP22 was scored according to the percentage of cells with positive nuclear staining and to the staining intensity. We assigned the percentage score as follows: 0 if no cell had nuclear staining, 1 if 0-25% of cells had nuclear staining, 2 if 25-50%, 3 if 50-75%, 4 if more than 75% of cells had nuclear staining. We scored the staining intensity as 0 for negative, 1 for weak, 2 for moderate, and 3 for strong. The total score was obtained by multiplying the percentage score by the intensity score. Two individuals who were both blinded to the slides examined and scored each sample. The final score was the mean value of the two scores provided by the individuals.

For immunofluorescence analysis of tissue sections, 15 frozen glioblastomas sections were fixed with paraformaldehyde and incubated with antibodies against KDM1A (ab90966, Abcam) and GSK3β (9315, Cell Signaling Technology) or KDM1A and USP22 (ab4812, Abcam) at 4°C overnight, followed by stained with Alexa Fluor 488 goat anti-rabbit IgG or Alexa Fluor 594 goat anti-mouse IgG for 1 hour at room temperature. Coverslips were mounted on slides using mounting medium with DAPI (H-1200, Vector Laboratories). Immunofluorescence images were acquired using a deconvolutional microscope (Zeiss). The percentages of nuclear GSK3β/KDM1A double stained cells and nuclear GSK3β negative but KDM1A positive cells were analyzed and compared in 5 random selected microscope fields of 15 specimens (75 microscope fields in total).

For immunofluorescence analysis of cultured cells, GSCs were grown on chamber slides precoated with poly (L-lysine). Cells were fixed with 4% paraformaldehyde, permeabilized with PBS containing 0.1% Triton X-100 for 5 min, and blocked with 1% BSA in PBS. Immunostaining was performed using the primary antibodies indicated in the related figures, and the above secondary antibodies.

Intracranial tumor cell injection

All animal experiments were approved by MD Anderson's Institutional Animal Care and Use Committee. The sample sizes of the animals were justified by statistical considerations and statistical power analyses. The animals were randomized to different experimental groups. The investigators were blinded to allocation during experiments and outcome assessment. GSC11 or GSC20 cells (5×10^5/mouse) were injected intracranially into 6- to 8-week-old male nude (nu/nu) mice (5 mice for each group) as described previously[52]. At the end of the experiments, the mice were humanely killed, and each mouse's brain was harvested, fixed in 4% formaldehyde, and embedded in paraffin. Tumor formation was determined by histologic analysis of tissue sections stained with hematoxylin and eosin. Tumor volumes were calculated using the formula $V= (\pi/6)\times a^2\times b$, where a and b are the tumor's short axis and long axis, respectively.

For in vivo therapeutic experiments, 1 d after intracranial implantation of tumor cells into nude mice (8 mice for each group), tideglusib (25 mg/kg/d) or TMZ (20 mg/kg/d) in a vehicle of dimethyl sulfoxide/polyethylene glycol 300 (Sigma, 1:4 ratio) was injected intraperitoneally every other day for 30 d. For combinatorial treatment, mice received injections of TMZ or tideglusib on alternating days for 30 d. The vehicle alone was used for the negative control group. In a set experiment to analyze mouse survival, animals were humanely killed when they were moribund; the remaining animals were humanely killed 90 d after tumor-cell injection.

Statistics and Reproducibility

We assessed differences in the human glioblastoma data using the Pearson correlation test, in the *in vitro* data using the two-tailed Student's *t*-test, and in the *in vivo* data using one-way analysis of variance. Survival analysis was conducted using the Kaplan-Meier model with a two-sided log-rank test. The results for statistical significance tests are included in the legend of each figure. The results in Fig.1e,f, Fig.3e, Fig.5a,b,d,h, Fig.7c-f, Supplementary Fig.2d, Supplementary Fig.3e,g, and Supplementary Fig.5a,i,j were independently performed for three times with similar results. *In vivo* mouse studies in Fig.6a,b contain 5 mice for each group, and were independently performed for two times with similar results. *In vivo* mouse studies in Fig.7d,f contain 8 mice for each group. The results in Supplementary Fig.1d and Supplementary Fig.7c were independently performed for two times. All other representative images have been independently reproduced three times with similar results. A P value of less than 0.05 was considered statistically significant.

Data availability

Source data for Fig.6a,b, Supplementary Fig. 1d, and Supplementary Fig.7c have been provided as Statistics Source Data (Supplementary Table 3). All data that support the conclusions are available from the authors on request, and/or available in the manuscript itself.

Supplementary Material

Refer to Web version on PubMed Central for supplementary material.

ACKNOWLEDGMENTS

We thank Joe Munch in MD Anderson's Department of Scientific Publications for editing the manuscript. We thank Dr. Yang Shi (Boston Children's Hospital) for providing Flag-KDM1A plasmid, Dr. Jianhua Yang (Texas Children's Cancer Center) for providing USP2, USP4, USP5, USP8, USP13, USP14, USP16, USP18, USP21, USP25, USP26, USP28, USP29, USP30, USP36, USP39, USP46, and USP48 expression plasmids, Dr. Hui-Kuan Lin (MD Anderson Cancer Center) for providing USP1, USP3, USP11, USP15, USP22, and CYLD expression plasmids, and Dr. Xi He (Boston Children's Hospital) for providing β-catenin$^{+/+}$ and β-catenin$^{-/-}$ MEFs. This work was supported in part by U.S. National Cancer Institute grants R01CA157933, R01CA182684, R01CA152309, P50CA127001, R01CA195651 and CA16672 (Cancer Center Support Grant).

REFERENCES

1. Cohen P, Frame S. The renaissance of GSK3. Nat Rev Mol Cell Biol. 2001; 2:769–776. [PubMed: 11584304]
2. Doble BW, Woodgett JR. GSK-3: tricks of the trade for a multi-tasking kinase. J Cell Sci. 2003; 116:1175–1186. [PubMed: 12615961]
3. Hoeflich KP, et al. Requirement for glycogen synthase kinase-3beta in cell survival and NF-kappaB activation. Nature. 2000; 406:86–90. [PubMed: 10894547]
4. Farago M, et al. Kinase-inactive glycogen synthase kinase 3beta promotes Wnt signaling and mammary tumorigenesis. Cancer Res. 2005; 65:5792–5801. [PubMed: 15994955]
5. Wang Z, et al. GSK-3 promotes conditional association of CREB and its coactivators with MEIS1 to facilitate HOX-mediated transcription and oncogenesis. Cancer Cell. 2010; 17:597–608. [PubMed: 20541704]
6. Naito S, et al. Glycogen synthase kinase-3beta: a prognostic marker and a potential therapeutic target in human bladder cancer. Clin Cancer Res. 2010; 16:5124–5132. [PubMed: 20889919]
7. Aberle H, Bauer A, Stappert J, Kispert A, Kemler R. beta-catenin is a target for the ubiquitin-proteasome pathway. EMBO J. 1997; 16:3797–3804. [PubMed: 9233789]
8. Sears R, et al. Multiple Ras-dependent phosphorylation pathways regulate Myc protein stability. Genes Dev. 2000; 14:2501–2514. [PubMed: 11018017]
9. Tang QL, et al. Glycogen synthase kinase-3beta, NF-kappaB signaling, and tumorigenesis of human osteosarcoma. J Natl Cancer Inst. 2012; 104:749–763. [PubMed: 22534782]
10. Miyashita K, et al. Potential therapeutic effect of glycogen synthase kinase 3beta inhibition against human glioblastoma. Clin Cancer Res. 2009; 15:887–897. [PubMed: 19188159]
11. Ougolkov AV, et al. Aberrant nuclear accumulation of glycogen synthase kinase-3beta in human pancreatic cancer: association with kinase activity and tumor dedifferentiation. Clin Cancer Res. 2006; 12:5074–5081. [PubMed: 16951223]
12. Ougolkov AV, Bone ND, Fernandez-Zapico ME, Kay NE, Billadeau DD. Inhibition of glycogen synthase kinase-3 activity leads to epigenetic silencing of nuclear factor kappaB target genes and induction of apoptosis in chronic lymphocytic leukemia B cells. Blood. 2007; 110:735–742. [PubMed: 17463171]
13. Reddiconto G, et al. Targeting of GSK3beta promotes imatinib-mediated apoptosis in quiescent CD34+ chronic myeloid leukemia progenitors, preserving normal stem cells. Blood. 2012; 119:2335–2345. [PubMed: 22262776]
14. Esteller M. Cancer epigenomics: DNA methylomes and histone-modification maps. Nat Rev Genet. 2007; 8:286–298. [PubMed: 17339880]
15. Hill EV, et al. Glycogen synthase kinase-3 controls IL-10 expression in CD4(+) effector T-cell subsets through epigenetic modification of the IL-10 promoter. Eur J Immunol. 2015; 45:1103–1115. [PubMed: 25627813]
16. Shi YJ, et al. Regulation of LSD1 histone demethylase activity by its associated factors. Mol Cell. 2005; 19:857–864. [PubMed: 16140033]
17. Wang Y, et al. LSD1 is a subunit of the NuRD complex and targets the metastasis programs in breast cancer. Cell. 2009; 138:660–672. [PubMed: 19703393]
18. Lv S, et al. LSD1 is required for chromosome segregation during mitosis. European journal of cell biology. 2010; 89:557–563. [PubMed: 20189264]

19. Kauffman EC, et al. Role of androgen receptor and associated lysine-demethylase coregulators, LSD1 and JMJD2A, in localized and advanced human bladder cancer. Mol Carcinog. 2011; 50:931–944. [PubMed: 21400613]
20. Hayami S, et al. Overexpression of LSD1 contributes to human carcinogenesis through chromatin regulation in various cancers. Int J Cancer. 2011; 128:574–586. [PubMed: 20333681]
21. Harris WJ, et al. The histone demethylase KDM1A sustains the oncogenic potential of MLL-AF9 leukemia stem cells. Cancer Cell. 2012; 21:473–487. [PubMed: 22464800]
22. Sareddy GR, et al. KDM1 is a novel therapeutic target for the treatment of gliomas. Oncotarget. 2013; 4:18–28. [PubMed: 23248157]
23. Suva ML, et al. Reconstructing and reprogramming the tumor-propagating potential of glioblastoma stem-like cells. Cell. 2014; 157:580–594. [PubMed: 24726434]
24. Gong AH, et al. FoxM1 Drives a Feed-Forward STAT3-Activation Signaling Loop That Promotes the Self-Renewal and Tumorigenicity of Glioblastoma Stem-like Cells. Cancer Res. 2015; 75:2337–2348. [PubMed: 25832656]
25. Rena G, Bain J, Elliott M, Cohen P. D4476, a cell-permeant inhibitor of CK1, suppresses the site-specific phosphorylation and nuclear exclusion of FOXO1a. EMBO Rep. 2004; 5:60–65. [PubMed: 14710188]
26. Adamo A, et al. LSD1 regulates the balance between self-renewal and differentiation in human embryonic stem cells. Nat Cell Biol. 2011; 13:652–659. [PubMed: 21602794]
27. Sun G, et al. Histone demethylase LSD1 regulates neural stem cell proliferation. Mol Cell Biol. 2010; 30:1997–2005. [PubMed: 20123967]
28. Dominguez JM, et al. Evidence for irreversible inhibition of glycogen synthase kinase-3beta by tideglusib. J Biol Chem. 2012; 287:893–904. [PubMed: 22102280]
29. Bolos M, Fernandez S, Torres-Aleman I. Oral administration of a GSK3 inhibitor increases brain insulin-like growth factor I levels. J Biol Chem. 2010; 285:17693–17700. [PubMed: 20351102]
30. Sereno L, et al. A novel GSK-3beta inhibitor reduces Alzheimer's pathology and rescues neuronal loss in vivo. Neurobiol Dis. 2009; 35:359–367. [PubMed: 19523516]
31. Chen J, et al. A restricted cell population propagates glioblastoma growth after chemotherapy. Nature. 2012; 488:522–526. [PubMed: 22854781]
32. Liu C, et al. Control of beta-catenin phosphorylation/degradation by a dual-kinase mechanism. Cell. 2002; 108:837–847. [PubMed: 11955436]
33. Gregory MA, Qi Y, Hann SR. Phosphorylation by glycogen synthase kinase-3 controls c-myc proteolysis and subnuclear localization. J Biol Chem. 2003; 278:51606–51612. [PubMed: 14563837]
34. Shin S, Wolgamott L, Yu Y, Blenis J, Yoon SO. Glycogen synthase kinase (GSK)-3 promotes p70 ribosomal protein S6 kinase (p70S6K) activity and cell proliferation. Proc Natl Acad Sci U S A. 2011; 108:E1204–1213. [PubMed: 22065737]
35. Kotliarova S, et al. Glycogen synthase kinase-3 inhibition induces glioma cell death through c-MYC, nuclear factor-kappaB, and glucose regulation. Cancer Res. 2008; 68:6643–6651. [PubMed: 18701488]
36. Beurel E, Jope RS. Differential regulation of STAT family members by glycogen synthase kinase-3. J Biol Chem. 2008; 283:21934–21944. [PubMed: 18550525]
37. Park BH, Qiang L, Farmer SR. Phosphorylation of C/EBPbeta at a consensus extracellular signal-regulated kinase/glycogen synthase kinase 3 site is required for the induction of adiponectin gene expression during the differentiation of mouse fibroblasts into adipocytes. Mol Cell Biol. 2004; 24:8671–8680. [PubMed: 15367685]
38. Foltz DR, Santiago MC, Berechid BE, Nye JS. Glycogen synthase kinase-3beta modulates notch signaling and stability. Current biology : CB. 2002; 12:1006–1011. [PubMed: 12123574]
39. Kubic JD, Mascarenhas JB, Iizuka T, Wolfgeher D, Lang D. GSK-3 promotes cell survival, growth, and PAX3 levels in human melanoma cells. Molecular cancer research : MCR. 2012; 10:1065–1076. [PubMed: 22679108]
40. Schaeffer V, et al. Binding of OTULIN to the PUB domain of HOIP controls NF-kappaB signaling. Mol Cell. 2014; 54:349–361. [PubMed: 24726327]

41. Elliott PR, et al. Molecular basis and regulation of OTULIN-LUBAC interaction. Mol Cell. 2014; 54:335–348. [PubMed: 24726323]
42. Wu Y, et al. The deubiquitinase USP28 stabilizes LSD1 and confers stem-cell-like traits to breast cancer cells. Cell Rep. 2013; 5:224–236. [PubMed: 24075993]
43. Zhang XY, et al. The putative cancer stem cell marker USP22 is a subunit of the human SAGA complex required for activated transcription and cell-cycle progression. Mol Cell. 2008; 29:102–111. [PubMed: 18206973]
44. Lin Z, et al. USP22 antagonizes p53 transcriptional activation by deubiquitinating Sirt1 to suppress cell apoptosis and is required for mouse embryonic development. Mol Cell. 2012; 46:484–494. [PubMed: 22542455]
45. Tolosa E, et al. A phase 2 trial of the GSK-3 inhibitor tideglusib in progressive supranuclear palsy. Mov Disord. 2014; 29:470–478. [PubMed: 24532007]
46. Persano L, et al. BMP2 sensitizes glioblastoma stem-like cells to Temozolomide by affecting HIF-1alpha stability and MGMT expression. Cell Death Dis. 2012; 3:e412. [PubMed: 23076220]
47. Kamnasaran D, Qian B, Hawkins C, Stanford WL, Guha A. GATA6 is an astrocytoma tumor suppressor gene identified by gene trapping of mouse glioma model. Proc Natl Acad Sci U S A. 2007; 104:8053–8058. [PubMed: 17463088]
48. Ligon KL, et al. Olig2-regulated lineage-restricted pathway controls replication competence in neural stem cells and malignant glioma. Neuron. 2007; 53:503–517. [PubMed: 17296553]
49. Hirose Y, Berger MS, Pieper RO. p53 effects both the duration of G2/M arrest and the fate of temozolomide-treated human glioblastoma cells. Cancer Res. 2001; 61:1957–1963. [PubMed: 11280752]
50. Schonberg DL, et al. Preferential Iron Trafficking Characterizes Glioblastoma Stem-like Cells. Cancer Cell. 2015; 28:441–455. [PubMed: 26461092]
51. Hu Y, Smyth GK. ELDA: extreme limiting dilution analysis for comparing depleted and enriched populations in stem cell and other assays. Journal of immunological methods. 2009; 347:70–78. [PubMed: 19567251]
52. Zhang N, et al. FoxM1 promotes beta-catenin nuclear localization and controls Wnt target-gene expression and glioma tumorigenesis. Cancer Cell. 2011; 20:427–442. [PubMed: 22014570]
53. Shembade N, Harhaj EW. Elucidating dynamic protein-protein interactions and ubiquitination in NF-kappaB signaling pathways. Methods Mol Biol. 2015; 1280:283–295. [PubMed: 25736755]
54. Li M, et al. Deubiquitination of p53 by HAUSP is an important pathway for p53 stabilization. Nature. 2002; 416:648–653. [PubMed: 11923872]

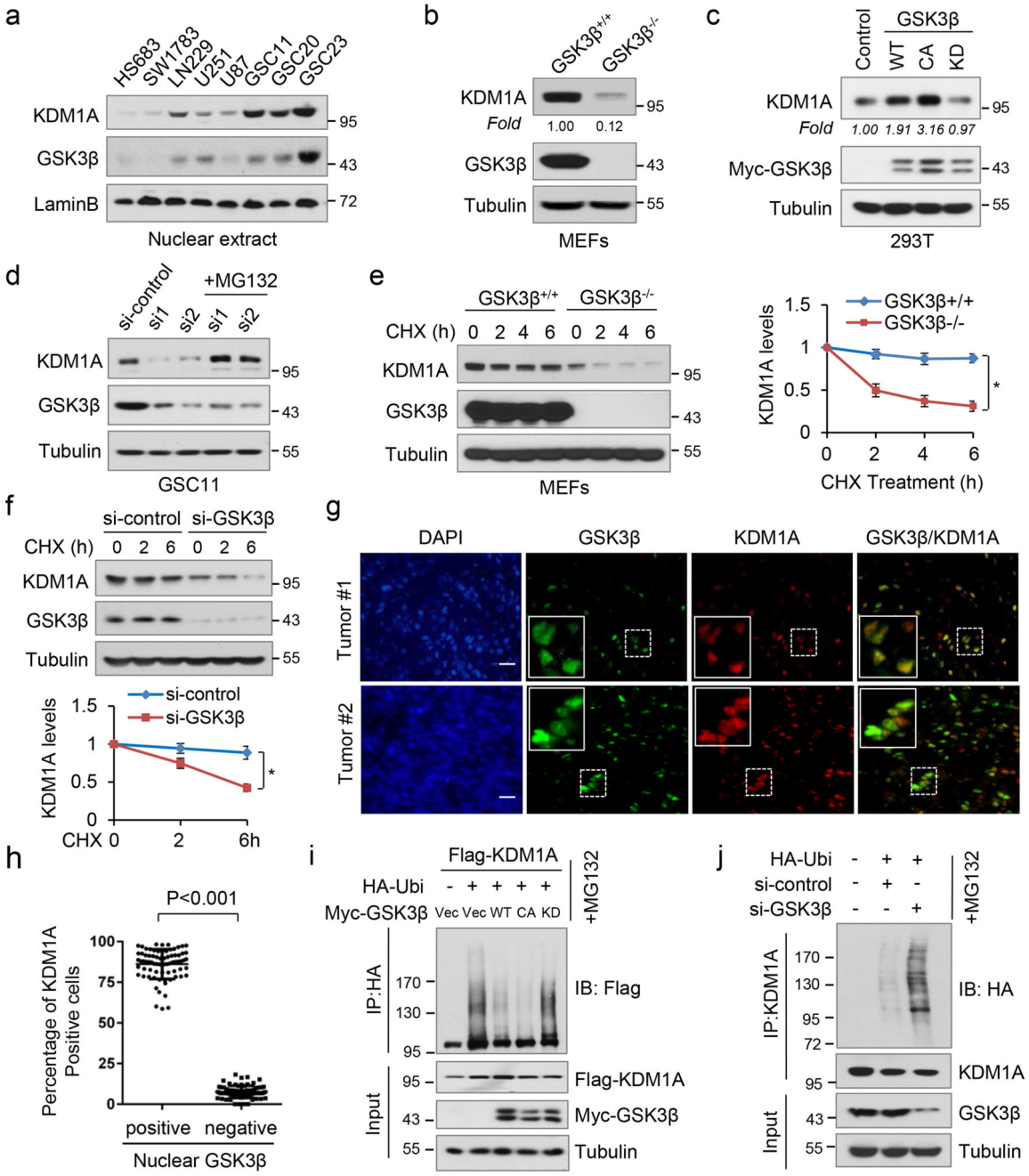

Figure 1. GSK3β stabilizes KDM1A by decreasing its ubiquitination

(**a**) Immunoblotting analysis of nuclear GSK3β and KDM1A in GSCs (GSC11, GSC20, and GSC23), glioblastoma cell lines (LN229, U251 and U87), and non-GSC glioma cell lines (HS683 and SW1783). (**b**) Immunoblotting analysis of KDM1A in GSK3β$^{+/+}$ or GSK3β$^{-/-}$ MEFs. KDM1A levels were quantified by scanning densitometry and the results are expressed as fold change relative to GSK3β$^{+/+}$ MEFs. (**c**) 293T cells were transfected with the indicated plasmids and KDM1A levels were assessed by immunoblotting. KDM1A fold changes were determined as in **b**. (**d**) GSC11 cells were transfected with GSK3β siRNAs

and then treated with or without 20 μM MG132 for 6h. Cell lysates were analyzed by immunoblotting. (**e**) GSK3β$^{+/+}$ or GSK3β$^{-/-}$ MEFs were treated with 50 μg/mL cycloheximide (CHX) for the indicated times and cell lysates were examined by immunoblotting (left panel). KDM1A band intensity was quantified and the results are expressed as KDM1A levels relative to untreated cells (mean ± s.d., n=3 independent experiments, paired Student's *t*-test, right panel). *P<0.01. (**f**) GSC11 cells were transfected with control or GSK3β siRNA and then treated with CHX as indicated. Western blot band intensity of KDM1A was quantified (mean ± s.d., n=3 independent experiments, paired Student's *t*-test, lower panel). *P<0.05. (**g**,**h**) Frozen tissue sections from human glioblastomas (n=15) were immunofluorescence double-stained with anti-KDM1A and anti-GSK3β antibodies. Representative images of two tumors are shown (**g**). Insets: high magnification images. Scale bar, 50 μm. In 5 random selected microscope fields of each tumor, the percentages of nuclear GSK3β/KDM1A double stained cells and nuclear GSK3β negative but KDM1A positive cells were analyzed and compared (mean ± s.d., n=75 microscope fields, unpaired Student's *t*-test). *P<0.001 (**h**). (**i**) 293T cells were transfected with the indicated plasmids and then treated with MG132. Cell lysates were immunoprecipitated by a HA-tag antibody and then analyzed by immunoblotting. (**j**) GSC11 cells were transfected with HA-Ubi plus control siRNAs or GSK3β siRNA and then treated with MG132. Cell lysates were immunoprecipitated using an anti-KDM1A antibody and then subjected to immunoblotting. Unprocessed original scans of blots are shown in Supplementary Fig. 8.

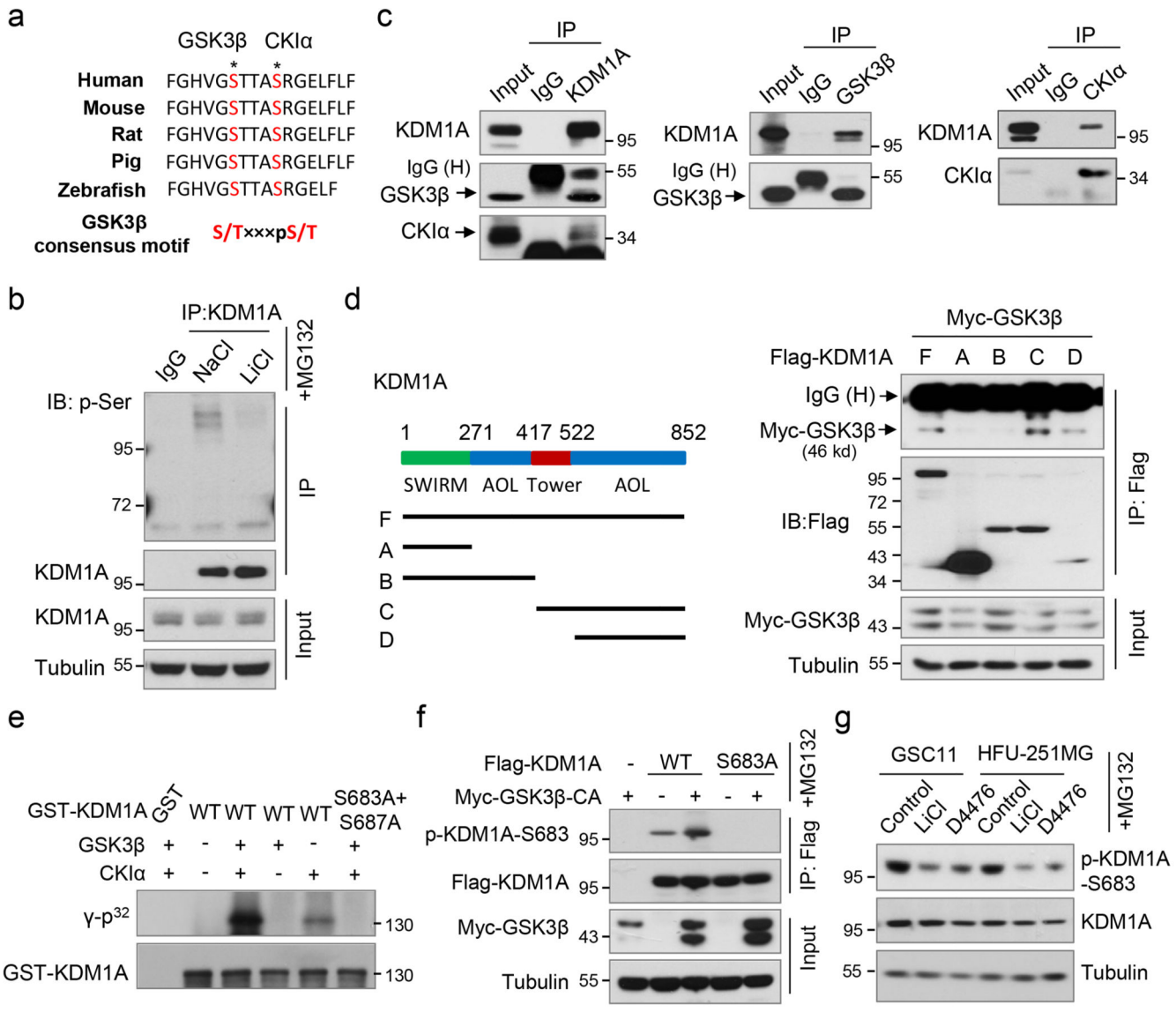

Figure 2. GSK3β phosphorylates KDM1A serine 683 after the phosphorylation priming by CK1α

(**a**) Amino acid sequence conservation in different species of the motif in KDM1A targeted by GSK3β. (**b**) GSC11 cells were treated with 20 mM sodium chloride or lithium chloride for 6 h in the presence of MG132. Cell lysates were immunoprecipitated using an anti-KDM1A antibody and then subjected to immunoblotting analysis using an anti-phospho-serine/threonine antibody. Normal rabbit immunoglobulin G (IgG) was used as the isotype control. (**c**) Reciprocal interaction of KDM1A with GSK3β and CK1α. GSC11 cell nuclear extracts were immunoprecipitated using antibodies against KDM1A, GSK3β, and CK1α, and then subjected to immunoblotting analysis. Inputs correspond to 5% nuclear extracts used for immunoprecipitation. IgG was used as the isotype control. (**d**) A series of KDM1A deletion constructs were co-transfected with the Myc-GSK3β plasmid into 293T cells. Cell lysates were immunoprecipitated using an anti-Flag antibody and then analyzed by immunoblotting. (**e**) *In vitro* kinase assays were performed by incubating purified active

GSK3β and/or CK1α with recombinant wild-type KDM1A or KDM1A S683A in the presence of [γ-^{32}P]ATP. The resultant products were subjected to SDS–polyacrylamide gel electrophoresis and autoradiography. (**f**) Flag-KDM1A-WT or Flag-KDM1A S683A was co-transfected with or without GSK3β-CA into 293T cells, and then treated with MG132 for 6h. Cell lysates were immunoprecipitated using an anti-Flag antibody and then analyzed by immunoblotting using a specific antibody against pKDM1A-S683. (**g**) GSC11 or HFU-251 MG cells were treated with lithium chloride or D4476 for 6 h in the presence of MG132, and the cell lysates were analyzed by immunoblotting using an antibody against pKDM1A-S683. Unprocessed original scans of blots are shown in Supplementary Fig. 8.

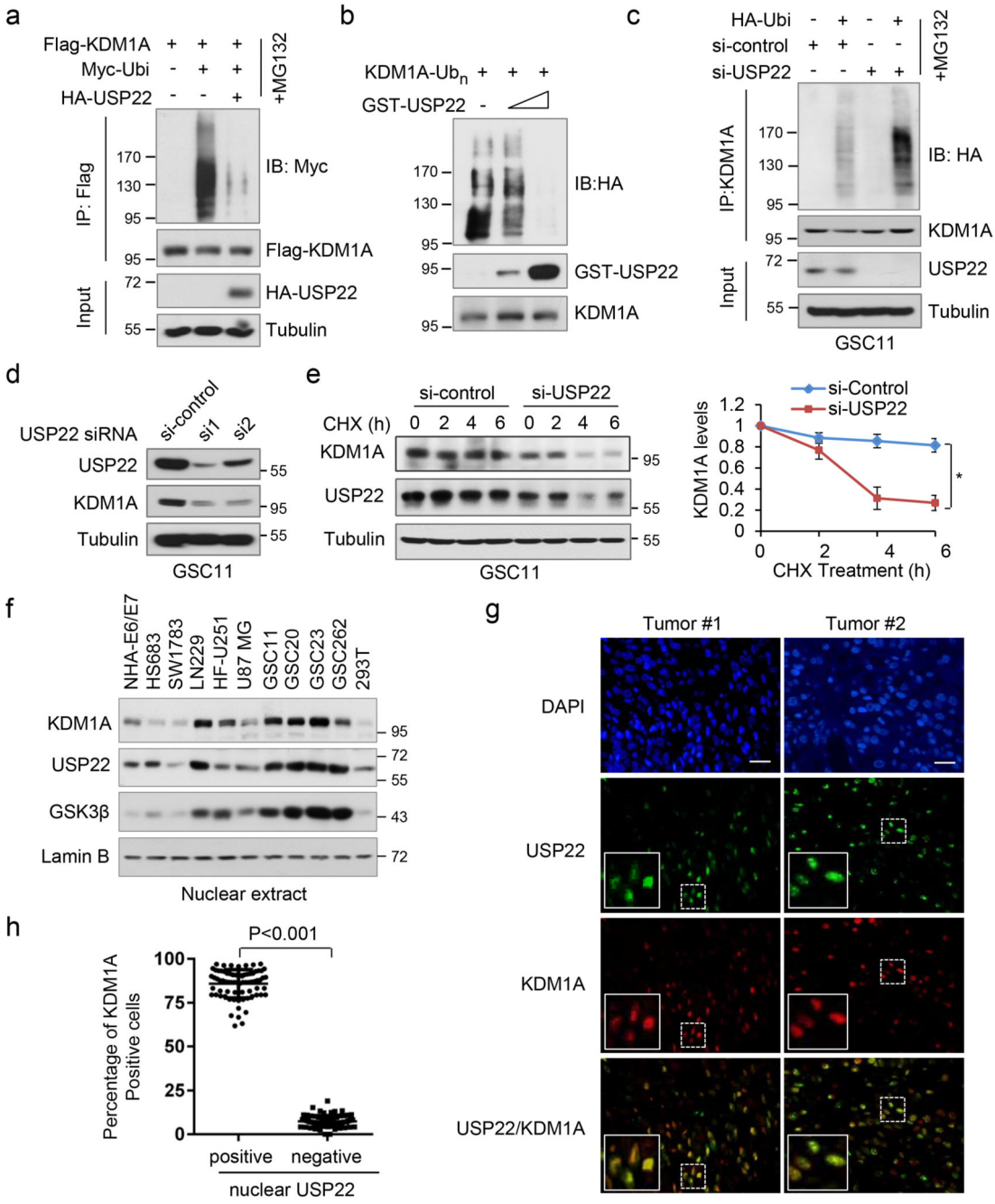

Figure 3. USP22 is a deubiquitinase of KDM1A

(**a**) 293T cells were transfected with the indicated plasmids and then treated with MG132 for 6 h. Cell lysates were immunoprecipitated using an anti-Flag antibody and then washed by ubiquitination wash buffer containing 1 M urea. The result immunoprecipitates were analyzed by immunoblotting. (**b**) HF-U251MG cells were transfected with Flag-KDM1A and HA-Ubi and then treated by MG132 for 6 h. Cell lysates were immunoprecipitated using an anti-Flag antibody. The purified KDM1A-Ub$_n$ was incubated with 10 ng or 100 ng recombinant GST-USP22 proteins in a deubiquitination buffer, and the result reactions were

subjected to immunoblotting analysis. (**c**) GSC11 cells were transfected with HA-Ubi plus control siRNA or USP22 siRNA. Cell lysates were immunoprecipitated using an anti-KDM1A antibody and then analyzed by immunoblotting. (**d**) GSC11 cells were transfected with two independent siRNAs targeting USP22, and levels of USP22 and KDM1A were detected by immunoblotting. (**e**) GSC11 cells were transfected with control siRNA or USP22 siRNA and then treated with CHX for the indicated times. Cell lysates were analyzed by immunoblotting (left panel). Band intensities of KDM1A were quantified and the results are expressed as KDM1A levels relative to untreated cells (mean ± s.d., n=3 independent experiments, paired Student's *t*-test, right panel). *P<0.01. (**f**) Immunoblotting analysis of the nuclear levels of GSK3β, USP22 and KDM1A in eleven cell lines. Quantification of western blot bands of each protein from three independent experiments was shown in Supplementary Fig.3h. (**g**,**h**) Frozen tissue sections from human glioblastomas (n=15) were stained as in Fig.1**g**, **h** with anti-KDM1A and anti-USP22 antibodies. Representative images of two tumors are shown (**g**). Scale bar, 50 μm. In 5 random selected microscope fields of each tumor, the percentages of nuclear USP22/KDM1A double stained cells and nuclear USP22 negative but KDM1A positive cells were analyzed and compared (mean ± s.d., n=75 microscope fields, unpaired Student's *t*-test). *P<0.001 (**h**). Unprocessed original scans of blots are shown in Supplementary Fig. 8.

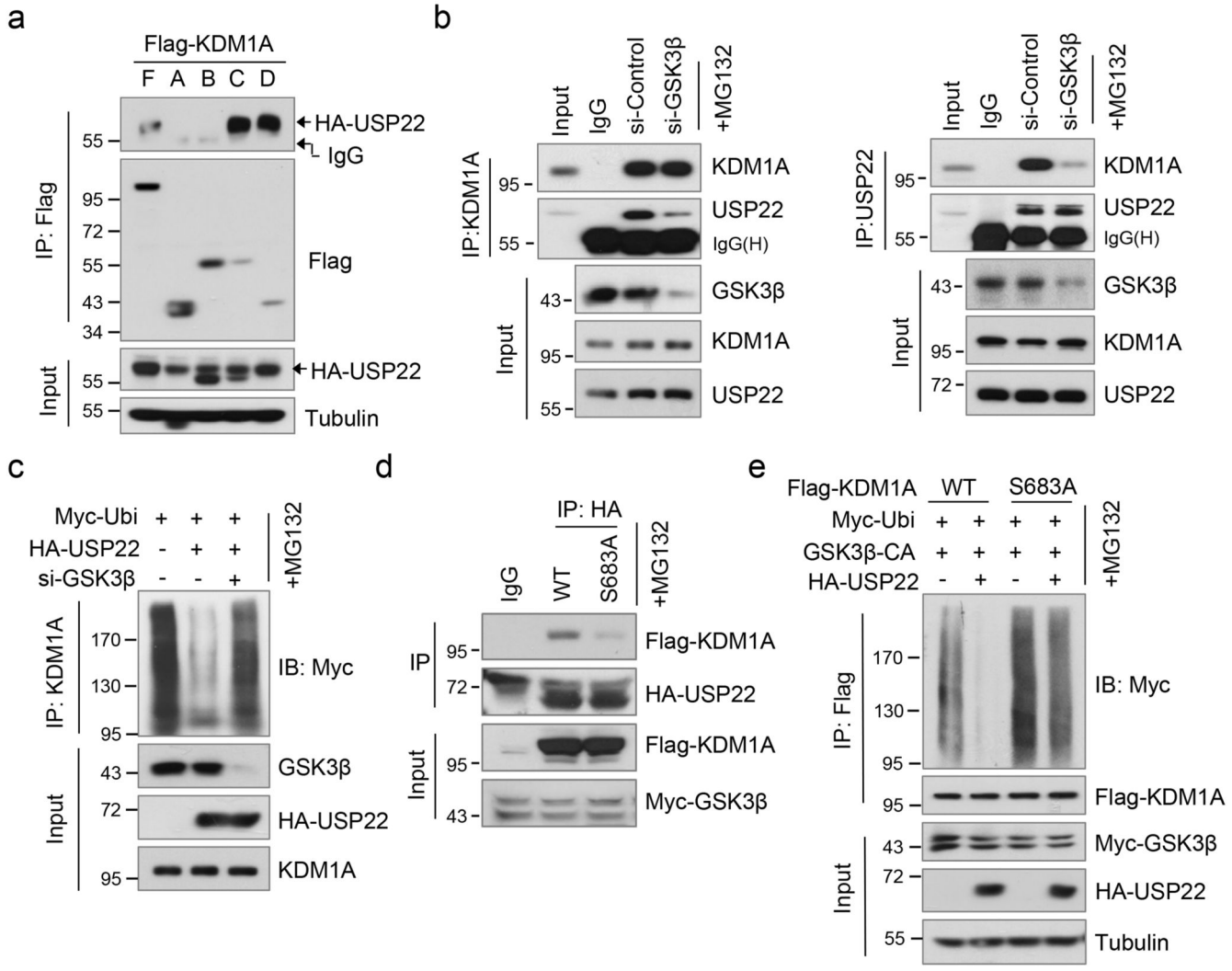

Figure 4. GSK3β promotes KDM1A's binding with and deubiquitination by USP22

(**a**) 293T cells were transfected with HA-USP22 and different KDM1A deletion constructs. Cell lysates were immunoprecipitated using an anti-Flag antibody and then analyzed by immunoblotting. (**b**) GSC11 cells were transfected with control siRNA or GSK3β siRNA for 36 h and then treated with 20 μM MG132 for 6h. Cell lysates were immunoprecipitated using an antibody against KDM1A (left panel) or USP22 (right panel) and then analyzed by immunoblotting. Inputs correspond to 2% of total cell lysates. Normal rabbit IgG was used as the isotype control. (**c**) GSC11 cells were transfected with Myc-Ubi and HA-USP22 plus control siRNA or GSK3β siRNA for 36 h. Then the cells were treated with MG132 for 6h. Cell lysates were immunoprecipitated using an anti-KDM1A antibody and then analyzed by immunoblotting. (**d**) 293T cells were transfected with HA-USP22, Myc-GSK3β-CA and Flag-KDM1A-WT or Flag-KDM1A S683A, and then treated with MG132 for 6h. Cell lysates were immunoprecipitated using an anti-HA antibody then analyzed by immunoblotting using an anti-Flag antibody. (**e**) 293T cells were transfected with Myc-Ubi, Myc-GSK3β-CA and Flag-KDM1A-WT or Flag-KDM1A S683A, and then treated with 20 μM MG132 for 6h. Cell lysates were immunoprecipitated using an anti-Flag antibody and

then analyzed by immunoblotting using an anti-Myc antibody. Unprocessed original scans of blots are shown in Supplementary Fig. 8.

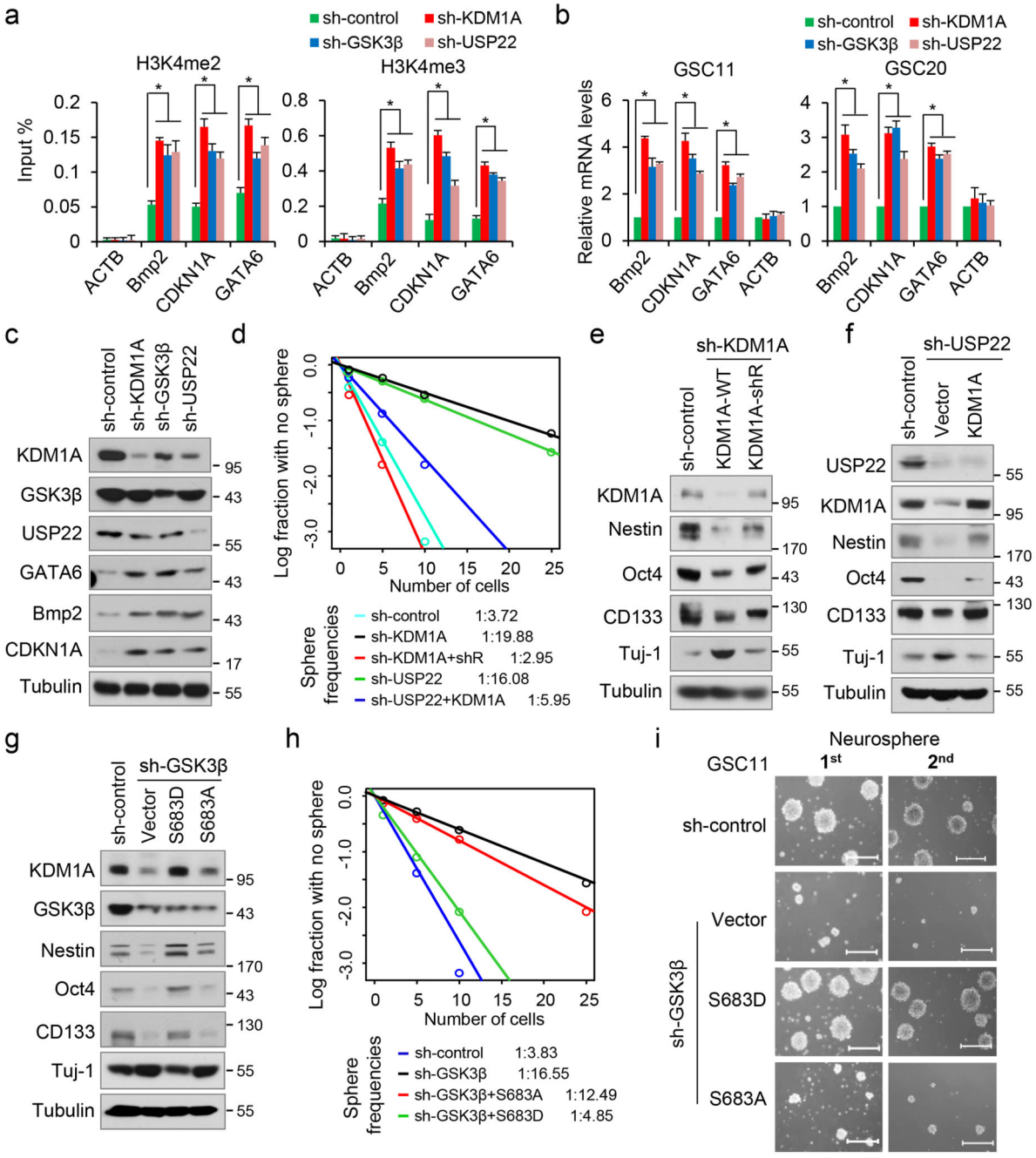

Figure 5. GSK3β and USP22 repress KDM1A target genes and are required for the maintenance of GSCs

(**a**) GSC11 cells were transfected with sh-Control, sh-KDM1A, sh-GSK3β, or sh-USP22 and ChIP assays were performed using an anti-H3K4me2/3 antibody. The immunoprecipitated DNA was analyzed by real-time PCR using specific primers in the promoter of *BMP2, CDKN1A,* or *GATA6. ACTB* promoter was used as a negative control. Values are the percentage to input (mean ± s.e.m., n=3 independent experiments, two-tailed Student's *t*-test). **P*<0.01. (**b**) *BMP2, CDKN1A*, and *GATA6* mRNA levels were analyzed

by real-time PCR in GSC11 and GSC20 cells stably expressing the indicated shRNAs. Values were normalized to that in control cells (mean ± s.e.m., n=3 independent experiments, two-tailed Student's *t*-test). *ACTB* was used as a negative control and *GAPDH* was used as an internal control. *P<0.01. (**c**) GSC11 cells stably expressing the indicated shRNAs were analyzed by immunoblotting using BMP2, CDKN1A, and GATA6 antibodies. (**d**) Limiting dilution assays (LDA) by plating decreasing number of GSC11 cells showed the frequencies of neurosphere formation. The frequencies of neurosphere formation were calculated as 1:x, where x is the average cell number. The significance of difference between the indicated groups was determined by Chi-square test (n=3 independent experiments). Sh-control vs sh-KDM1A, P=2.39e-13; sh-KDM1A vs sh-KDM1A+shR, P=5.36e-13; sh-control vs sh-USP22, P=5.55e-11; sh-USP22 vs sh-USP22+KDM1A, P=1.85e-05. (**e**) GSC11 cells expressing KDM1A shRNA were reconstituted by the expression of shRNA-resistant KDM1A (KDM1A-shR). (**f**) GSC11 cells expressing USP22 shRNA were reconstituted by the expression of wild-type KDM1A. (**g**) GSC11 cells expressing GSK3β shRNA were reconstituted by the expression of KDM1A S683D or KDM1A S683A. Cell extracts in **e-g** was assessed by immunoblotting. (**h**) LDA analysis of GSC11 cells showed the frequencies of neurosphere formation. The significance of difference between the indicated groups was determined by Chi-square test (n=3 independent experiments). Sh-control vs sh-GSK3β, P=8.9e-11; sh-GSK3β vs GSK3β+S683D, P=6.54e-08, sh-GSK3β vs GSK3β+S683A, P=0.215. (**i**) Representative photographs of primary (1st) or secondary (2nd) neurosphere formation of GSC11 cells expressing sh-Control, sh-GSK3β, sh-GSK3β +KDM1A S683D, or sh-GSK3β+KDM1A S683A. Scale bar, 500μm. Unprocessed original scans of blots are shown in Supplementary Fig. 8.

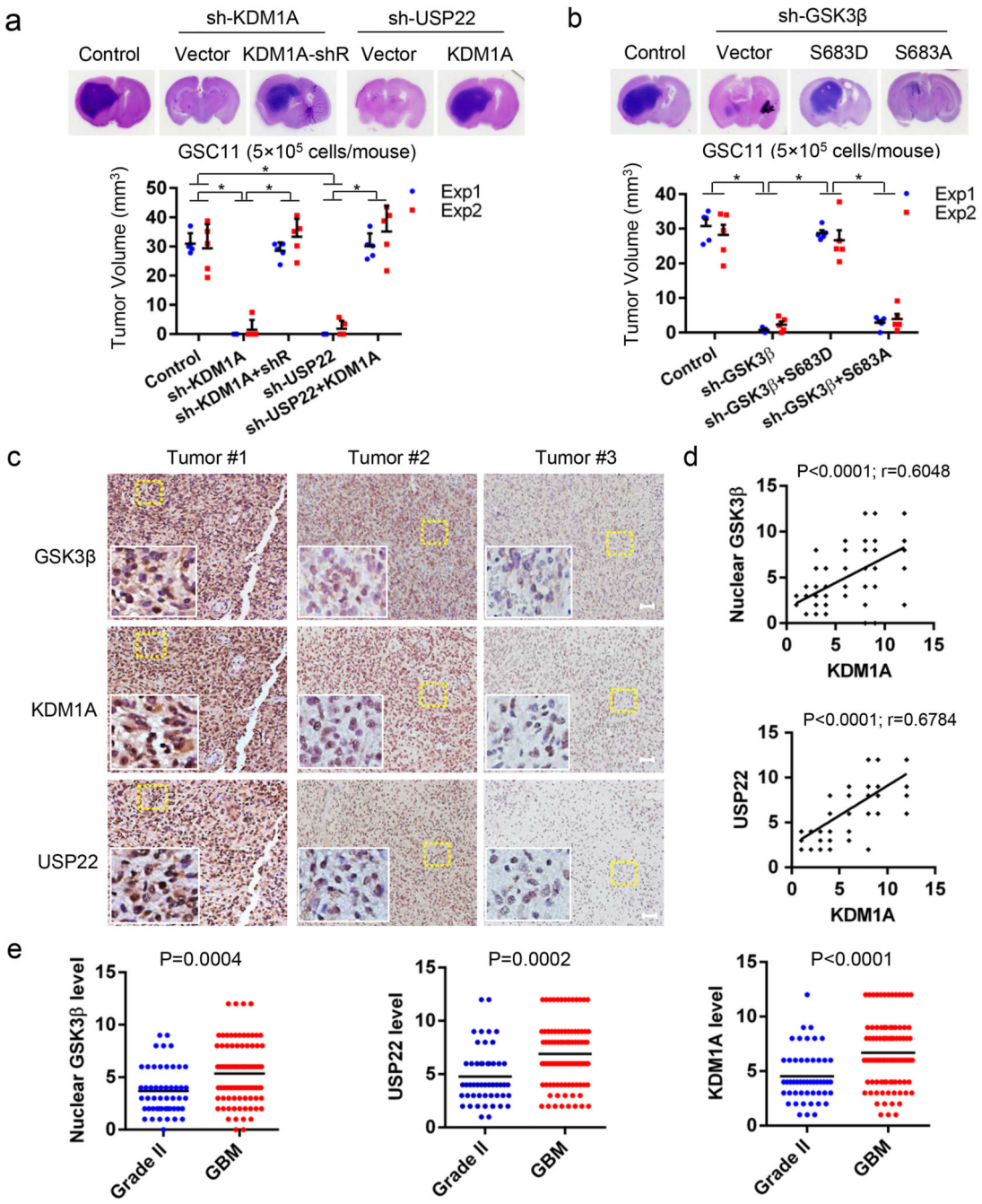

Figure 6. GSK3β-USP22-KDM1A axis is required for gliomagenesis of GSCs and associated with grade of glioma malignance in human glioma specimens

(**a**) GSC11 cells (5×10^5 cells/mouse) stably expressing sh-Control, sh-KDM1A, sh-KDM1A +KDM1A-shR, sh-USP22, or sh-USP22+KDM1A-WT were intracranially injected into nude mice. (**b**) GSC11 cells expressing sh-Control, sh-GSK3β, sh-GSK3β+KDM1A S683D, or sh-GSK3β+KDM1A S683A were intracranially injected into nude mice. In **a** and **b**, six weeks after injection, the mice were humanely killed, and tumor growth was assessed. The hematoxylin and eosin-stained sections show representative tumor xenografts. Tumor

volumes were calculated (mean ± s.d., n=5 mice for each group, One-way ANOVA test). Data show two independent experiments (Exp1 and Exp2). *P<0.001. (**c**,**d**) Immunohistochemistry assays using anti-GSK3β, anti-KDM1A, and anti-USP22 antibodies were performed on 95 human glioblastoma specimens. Representative images of three tumors are shown. Insets: high magnification images corresponding to the areas marked by yellow dot lines (**c**). Scale bar, 100 μm. Staining of nuclear GSK3β, KDM1A, or USP22 was scored on a scale of 1–12. The correlation of nuclear GSK3β, KDM1A, and USP22 was statistically significant among different specimens (n=95 glioblastomas, top panel, r=0.6048, P<0.001; bottom panel, r=0.6784, P<0.001; Pearson correlation test). Note that the scores of some samples overlap (**d**). (**e**) Immunohistochemistry analysis of the expression of GSK3β, anti-KDM1A, and anti-USP22 in human glioma specimens. Human grade II astrocytoma specimens (n=50) were immunohistochemically stained with anti-KDM1A, USP22 or GSK3β antibody, and expression scores of KDM1A, USP22 or nuclear GSK3β were compared with those in 95 glioblastoma (GBM) specimens as in (**d**) (n=50 astrocytomas and n=95 glioblastomas, unpaired Student's *t*-test). Source data of Fig. 6a,b can be found in Supplementary Table 3.

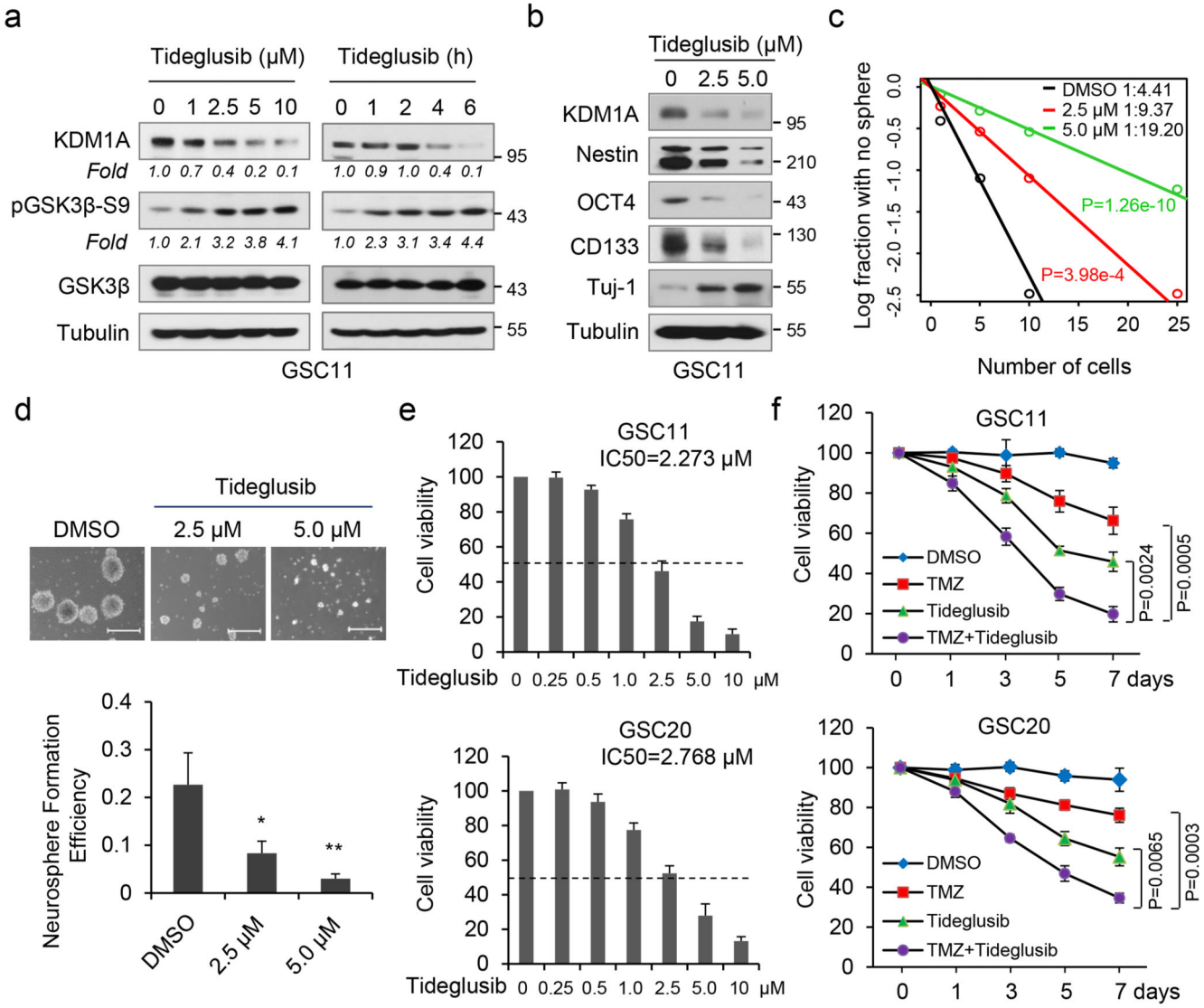

Figure 7. The GSK3 inhibitor tideglusib attenuates GSC self-renewal and enhances the effect of TMZ on GSC proliferation

(**a**) GSC11 cells were treated with the indicated concentrations of tideglusib for 6 h (left panel) or with tideglusib at a final concentration of 5 μM for the indicated times (right panel). Cell lysates were analyzed by immunoblotting using the indicated antibodies. Data were quantified and the results are expressed as fold change relative to control cells. (**b**) GSC11 cells were treated with 2.5 μM or 5 μM tideglusib for 36 h, and cell lysates were assessed by immunoblotting. (**c**) ELDA by plating decreasing number of GSC11 cells showed the frequencies of neurosphere formation in GSC11 cell treated with 2.5 μM or 5 μM tideglusib. DMSO vehicle was used as a control. The significance of difference between the indicated groups was determined by Chi-square test (n=3 independent experiments). (**d**) Primary neurosphere formation were assessed in GSC11 cells treated with 2.5 μM or 5 μM tideglusib for 10 d. Representative images are shown (upper panel). Scale bar: 500μm. Neurosphere formation efficiency (spheres/cells plated) was quantified (lower panel, mean ±

s.e.m., n=3 independent experiments, two-tailed Student's *t*-test). *P<0.01, ** P<0.001. (**e**) GSC11 and GSC20 cells were treated with different concentration of tideglusib for 7d. IC50 values for each cell line were calculated using the GraphPad Prism 6 software (mean ± s.e.m., n=3 independent experiments). (**f**) GSC11 and GSC20 cells were treated with dimethyl sulfoxide (DMSO), temozolomide (TMZ; 100 μM), tideglusib (2.5 μM), or TMZ plus tideglusib for the indicated times, and cell proliferation was assessed by XTT assays (mean ± s.e.m., n=3 independent experiments, paired Student's *t*-test). P values were analyzed by comparing TMZ or tideglusib along versus the combination of the two and shown. Unprocessed original scans of blots are shown in Supplementary Fig. 8.

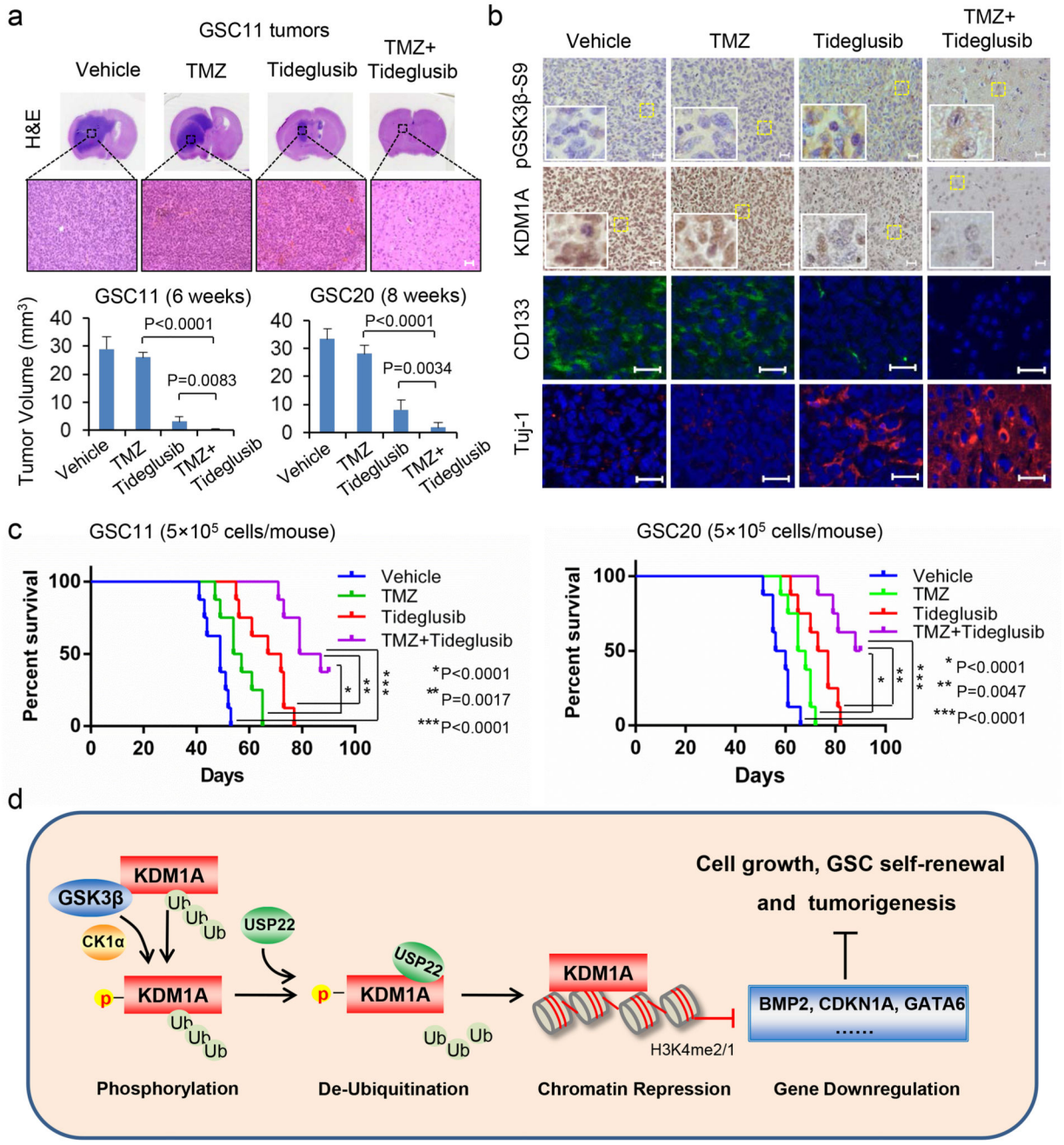

Figure 8. Tideglusib attenuates the tumor-initiating ability of GSCs and sensitizes GSCs-derived xenografts to TMZ

(**a**) GSC11 or GSC20 cells (5×10^5 cells/mouse) were intracranially injected into nude mice. One day after cell injection, mice were intraperitoneally injected with TMZ (20 mg/kg/d) or tideglusib (25 mg/kg/d) every other day for 30d. For combinatorial treatment, mice received injections of TMZ or tideglusib on alternating days for 30 d. Mice were humanely killed 6 weeks after the injection of GSC11 cells or 8 weeks after the injection of GSC20 cells. H&E stained sections show representative tumor xenografts. Scale bar, 50μm. Tumor volumes

were calculated (mean ± s.d., n=8 mice for each group, One-way ANOVA test). (**b**) Consecutive sections from tumor xenografts derived from GSC11 cells were immunostained using the indicated antibodies. Representative microphotographs of immunostaining for each group are shown. Insets: high magnification images corresponding to the areas marked by yellow dot lines. Scale bar (IHC and IF), 50 μm. (**c**) GSC11 or GSC20 cells (5×10^5 cells/mouse) were intracranially injected into nude mice. Mice were treated as in **a**. The survival of mice was evaluated (n = 8 mice for each group, Kaplan-Meier model with two-sided log-rank test). P values were analyzed by comparing TMZ or tideglusib along versus the combination of the two. (**d**) Illustration of the GSKβ-USP22-KDM1A axis in the regulation of tumorigenesis. Nuclear GSKβ phosphorylates KDM1A after the priming phosphorylation by CK1α. KDM1A phosphorylation enhances its binding and deubquitination by USP22, leading to KDM1A stabilization. GSK3β-dependent stabilization of KDM1A promotes the demethylation of histone H3K4 and represses the transcription of *BMP2*, *CDKN1A*, and *GATA6*, which in turn promotes glioblastoma tumorigenesis.